ROYAL SOCIETY
OF CHEMISTRY

Check for updates

NiFe$_2$O$_4$ nanoparticles: an efficient and reusable catalyst for the selective oxidation of benzyl alcohol to benzaldehyde under mild conditions†

Saddam Iraqui, Siddhartha Shankar Kashyap and Md. Harunar Rashid [ID] *

Benzaldehyde is one of the most important and versatile organic chemicals for industrial applications. This study explores a milder approach for the fabrication of NiFe$_2$O$_4$ nanoparticles (NPs) for use as a catalyst in the selective oxidation of benzyl alcohol to benzaldehyde. A co-precipitation method coupled with hydrothermal aging has been adopted to synthesize NiFe$_2$O$_4$ NPs in the absence of any additive. Different techniques such as electron microscopy, diffractometry, and photoelectron spectroscopy have been used to characterize the products. The results showed that the synthesized NiFe$_2$O$_4$ NPs are spherical, pure, and highly crystalline with sizes below 12 nm possessing superparamagnetic behaviour. The catalytic activity of the synthesized NiFe$_2$O$_4$ NPs has been assessed in the selective oxidation of benzyl alcohol under ambient reaction conditions. A conversion of 85% benzyl alcohol with 100% selectivity has been attained with *t*-butyl hydroperoxide at 60 °C in 3 h. With the optimized reaction conditions, the generality of the newly developed protocol has been expanded to a wide array of substituted benzyl alcohols with good performance. The NiFe$_2$O$_4$ nanocatalysts are magnetically separable and are reusable up to five cycles without loss of catalytic activity.

1. Introduction

Ferrites are categorized as electro-ceramics with ferromagnetic properties, mainly consisting of ferric oxide, α-Fe$_2$O$_3$.[1] The general formula of ferrites is represented by $(M_{1-x}Fe_x)_A$ $(M_x$-Fe$_{2-x})_B$O$_4$, where A and B represent tetrahedral and octahedral sites respectively.[2] Magnetic ferrites are inverse spinel where the divalent ions occupy the octahedral sites and the trivalent ions occupy both the octahedral and tetrahedral sites giving rise to various magnetic behaviors.[2] Both the structural and magnetic properties of ferrites vary depending on their sizes. Nickel ferrite (NiFe$_2$O$_4$) is a cubic ferrimagnetic oxide with an inverse structure where the divalent ion (Ni^{2+}) occupies the octahedral sites and the trivalent ions (Fe^{3+}) occupy both the tetrahedral and octahedral sites.[3] The ferrimagnetism arises from the magnetic moment of the inverted spins present between the Fe^{3+} ions in the tetrahedral sites and Ni^{2+} ions in the octahedral sites.[2] So, NiFe$_2$O$_4$ is considered as a soft ferromagnetic material.[4] It is reported that when the diameter of the particle is less than that of a single magnetic domain, spinel ferrite nanoparticles (NPs) become superparamagnetic.[4] Among different ferrites, spinel NiFe$_2$O$_4$ became a topic of interest in recent times because of its excellent technological applications.[5–9]

These technological applications motivated researchers to develop an efficient chemical technique to synthesize NiFe$_2$O$_4$ of controlled sizes and shapes. Among different chemical synthesis methods, the hydrothermal method is considered to be the most efficient because of various advantages associated with such techniques such as well-controlled particle size, morphology, and crystallinity. Also by changing the reaction time, pH of the reaction medium, and temperature, highly crystallized and weakly accumulated powders having narrow size distributions can be produced.[10,11] Moreover, hydrothermal methods are simple, environment-friendly, and cost-effective.[4,12] Accordingly, many researchers utilized the hydrothermal method under different reaction conditions to synthesize NiFe$_2$O$_4$ NPs. For example, Shen *et al.* reported the synthesis of highly ordered octahedral like NiFe$_2$O$_4$ with enhanced magnetic performance *via* a novel multistep hydrothermal approach at 180 °C for 8 h in the presence of ethylene glycol.[13] Kesavan *et al.* synthesized NiFe$_2$O$_4$ NPs with a cubic crystal structure with an average crystallite size of 16 nm by a hydrothermal method at 130 °C for 12 h in the presence of polyvinylpyrrolidone (PVP) as an additive. They further calcined the isolated sample at 550 °C for 4 h to get the desired product.[14] Safaei *et al.* presented a simple and efficient method to synthesize a magnetic NiFe$_2$O$_4$ nanocatalyst under hydrothermal conditions at 200 °C for 24 h using urea and polyethylene glycol (PEG) as additives.[15] Paul *et al.* reported a novel and facile approach for the synthesis of spinel NiFe$_2$O$_4$ NPs employing homogeneous chemical precipitation followed by

Department of Chemistry, Rajiv Gandhi University, Rono Hills, Doimukh 791 112, Arunachal Pradesh, India. E-mail: harunar.rashid@rgu.ac.in

hydrothermal treatment using tributylamine (TBA) as a hydroxylating agent in the presence of PEG as a surfactant.[16] Karaagac et al. synthesized $NiFe_2O_4$ NPs of different sizes and shapes in a two-step co-precipitation/hydrothermal process by varying the temperature between 125 and 200 °C for 40 h.[17] Li et al. reported the synthesis of nanocrystalline $NiFe_2O_4$ via a hydrothermal method at 160 °C for 6 h assisted with homogeneous co-precipitation at low temperatures in the presence of urea.[18] There was no defined morphology and size of the formed $NiFe_2O_4$ nanocrystal. Rafique et al. reported the synthesis of $NiFe_2O_4$ nanooctahedra in the gram scale via a hydrothermal method at 220 °C for 12 h.[19] Nejati et al. reported the synthesis of $NiFe_2O_4$ NPs by a hydrothermal method at different temperatures of 100, 130, and 150 °C for 18 h.[20] They used triethylamine in ethyl acetate solution to adjust the pH of the reaction mixture. They further investigated the inhibition of the surfactant (glycerol or sodium dodecyl sulphate) on particle growth. Although the above reports were of successfully synthesized $NiFe_2O_4$ NPs, most of the reports utilized additives in the form of surfactants or polymers or the reaction was performed at higher temperatures or the reaction was continued for a long time. So, the processes are lengthy, energy-consuming, and in some cases complex due to the presence of additives. Hence, a mild and simple hydrothermal method of synthesis of uniform $NiFe_2O_4$ NPs without using any additive is highly desirable and is the current topic of research interest.

One of the most important and versatile organic chemicals in the chemical industry is benzaldehyde. It serves as a synthetic intermediate for agrochemicals, dyes, perfumery, and pharmaceuticals.[21] It appears as the second most important aromatic molecule after vanillin used in the cosmetics and flavour industries.[22,23] In commercial practice, benzaldehyde is commonly prepared by the partial oxidation of benzyl alcohol, alkaline hydrolysis of benzyl chloride, liquid-phase oxidation of toluene, and the carbonylation of benzene.[24,25] However, the existence of a chlorinated product and low selectivity towards benzaldehyde are the main concerns of these processes.[26] Another method to produce benzaldehyde is through the catalytic oxidation of styrene at the side chain.[27] However, the harsh reaction conditions and complex and expensive methodologies implemented for the controlled conversion of styrene into one desired oxygenated product (selectivity issue) limit the applicability of this method. Therefore, many new routes have been introduced in recent years for the synthesis of benzaldehyde. One of the popular techniques is the catalytic oxidation of benzyl alcohol selectively using both homogeneous and heterogeneous catalyst systems.[28] Although homogeneous systems were found to be successful, reusability, cost, sustainability, and toxicity issues limit their uses.[28] Whereas, heterogeneous catalysts are in general more favourable than traditional homogeneous ones due to their promising easy separation and potential recycling. Subsequently, several heterogeneous catalyst systems were reported recently for the oxidation of benzyl alcohol with different oxidants. But satisfactory results in terms of selectivity were attained in only a few cases.[29–34] Therefore, the demand for efficient and selective catalysts is the driving force for the researchers to synthesize

new catalysts. Among different heterogeneous catalysts, magnetic ferrites occupied a significant position due to their easy recovery, low cost, and low toxicity. For example, Gawande et al. reported the use of recyclable Fe_3O_4–Co NPs for the oxidation of alcohols to carbonyl compounds using t-butyl hydroperoxide (TBHP) as the oxidant. They attained a conversion of 82% benzyl alcohol to benzaldehyde at 80 °C after 5 h.[35] Saranya et al. reported the use of supported $NiFe_2O_4$ for the oxidation of benzyl alcohol in an acetonitrile medium at 80 °C using O_2 as the oxidant. The conversion of benzyl alcohol reached a maximum of 77% with 100% selectivity.[36] Sadri et al. reported the use of the magnetically separable nano-$CoFe_2O_4$ catalyst for oxidation of primary and secondary benzylic and aliphatic alcohols to produce the corresponding carbonyl products in water with oxone as the oxidizing agent at room temperature.[37] Zhu et al. reported the use of $CuFe_2O_4$ as a catalyst for the oxidation of benzyl alcohol in the presence of TEMPO in water at 100 °C for 24 h using O_2 as the oxidant. They recorded a maximum yield of 95%, which decreased when the amount of TEMPO was lowered.[38] Bhat et al. reported the use of different ferrites for the oxidation of benzyl alcohol in an acetonitrile medium using H_2O_2 as an oxidant at 80 °C for 7 h. The maximum conversion of 82.4% was attained with a nano-functionalized $NiFe_2O_4$ catalyst.[39] Nasrollahzadeh et al. studied the performance of $CoFe_2O_4$ NPs in the oxidation of benzyl alcohol to benzaldehyde using H_2O_2 as an oxidant under solvent-free conditions. They acquired >99% conversion of benzyl alcohol to benzaldehyde at 110 °C for 5 h.[40] A careful investigation suggests that in the above reports either the catalyst system was prepared using a complex methodology or harsh conditions such as high temperatures or longer reaction time was applied for the desired conversion. So, it is highly desirable to design and develop an efficient and mild protocol for the selective oxidation of benzyl alcohol to benzaldehyde. To address the above issues with the synthesis of ferrites and the selective oxidation of benzyl alcohol, the objective of the current investigation is (i) to synthesize uniform, easily separable, and cost-effective non-toxic catalysts easily and simply and (ii) to use the synthesized catalyst for selective oxidation of benzyl alcohol to benzaldehyde under mild reaction conditions. Subsequently, we were able to address some of the issues by synthesizing $NiFe_2O_4$ NPs via coprecipitation coupled with hydrothermal treatment in the absence of any additive or other toxic agents at a temperature of 180 °C for 3 h. We were able to produce highly crystalline, uniform particles. These particles successfully catalyze the oxidation of benzyl alcohol and its substituted derivative selectively under mild conditions. So, the objective of the research was accomplished with great success.

2. Experimental section

2.1 Chemicals

Anhydrous ferric chloride ($FeCl_3$), nickel chloride hexahydrate ($NiCl_2 \cdot 6H_2O$), benzyl alcohol ($C_6H_5CH_2OH$), hydroquinone, and ammonium hydroxide (NH_4OH; 25%) were purchased from Merck India. t-Butyl hydroperoxide (TBHP; 70% in water) and other substituted benzylic and aliphatic alcohols were

purchased from Sigma-Aldrich and Alfa-Aesar with the purity of 97–99%. All the reagents were used without further purification. All the glassware was cleaned in a bath of freshly prepared aqua-regia solution (HCl : HNO_3 = 3 : 1 V/V) and then rinsed thoroughly with double distilled water. Double distilled water was used for all types of material preparation.

2.2 Synthesis of $NiFe_2O_4$ nanoparticles

To synthesize $NiFe_2O_4$, equal volume of aqueous $NiCl_2$ (25 mL; 0.05 M) and $FeCl_3$ (25 mL; 0.1 M) solution were taken in a round bottom (RB) flask fitted with a condenser and placed at 80 °C to get a Ni^{2+} to Fe^{3+} ratio of 1 : 2. The mixture of metal salt solutions was then subjected to constant stirring to get a homogeneous solution followed by the dropwise addition of aqueous NH_4OH (5.25 M; 20 mL) solution. The reaction mixture was stirred for 30 min at the same temperature. The color of the reaction mixture gradually changed and finally, a reddish-brown precipitate was noticed. The whole reaction mixture was then transferred into a 100 mL Teflon lined autoclave and aged for 3 h at 180 °C. After that, the reactor containing the product was allowed to cool down to room temperature naturally. The solid precipitate was collected by magnetic separation using a simple bar magnet. The isolated solid product was purified by washing with H_2O several times till a pH of 7.0 was obtained and finally dried in a vacuum at 60 °C for 12 h. This sample was labelled as $NiFe_2O_4$-3. Another set of the reaction was carried out by changing the hydrothermal aging time to 4 h keeping all the reaction conditions the same as the previous one and the sample was denoted as $NiFe_2O_4$-4. The synthesized particles were characterized by different spectroscopic, microscopic, and diffractometric techniques as discussed in detail in the ESI.†

2.3 General procedure for the oxidation of benzyl alcohol

For the oxidation reaction, 10 mg of $NiFe_2O_4$ NPs (0.04 mmol; sample $NiFe_2O_4$-3) was added to 3 mL of acetonitrile taken in a clean dry round bottom flask of volume 10 mL. For the efficient dissolution of the catalyst, the mixture was sonicated for about 5 min. Following this, 0.104 mL benzyl alcohol (1 mmol) and 0.05 mL of 70% TBHP (0.4 mmol) was added to the reaction mixture and was subjected to magnetic stirring at 60 °C under reflux conditions. The progress of the reaction was monitored by thin-layer chromatography (TLC). After the complete conversion of the reaction, the reaction mixture was allowed to cool to room temperature and the catalyst was separated using a simple bar magnet. The reaction mixture was then diluted with an optimum amount of ethyl acetate and water. The organic layer was separated and washed with brine and dried over Na_2SO_4. The solvent was removed in a rotary evaporator (Buchi) under reduced pressure. The crude product was purified by column chromatography (5% ethyl acetate in hexane) on silica gel (100–200 mesh) to get the desired product. The products were identified by ^1H NMR and ^{13}C NMR.
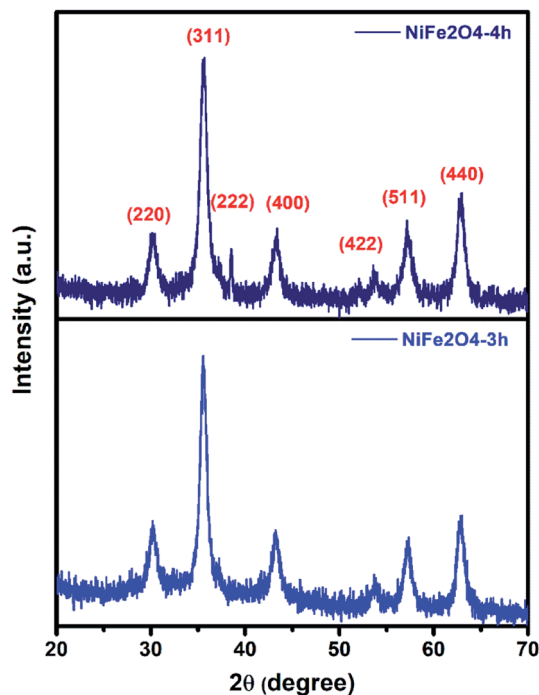

Fig. 1 XRD patterns of $NiFe_2O_4$ NPs prepared at the hydrothermal aging time of 3 and 4 h.

3. Results and discussion

3.1 X-ray diffraction study

Fig. 1 shows the X-ray diffraction (XRD) pattern of the as-prepared samples. The diffractogram showed diffraction peaks at 2θ = 30.1, 35.6, 37.2, 43.2, 53.7, 57.1, and 62.7° which are assigned to (220), (311), (222), (400), (422), (511), and (440) planes of cubic structures of spinel $NiFe_2O_4$ (JCPDS Card no. 10-0325).[41] No additional diffraction peaks due to impurities were noticed in the XRD pattern indicating the formation of pure and highly crystalline spinel $NiFe_2O_4$. Similar XRD results were reported earlier for both spherical and sheet-like $NiFe_2O_4$ NPs.[4,42] The average crystallite size as measured using Scherer's equation (eqn (1)) was found to be 8.2 nm for both the samples.

$$D = \frac{0.9\lambda}{\beta \cos\theta} \tag{1}$$

where λ is the wavelength of the X-ray radiation (0.154 nm), θ is the diffraction angle and β is the full width at half maximum (FWHM).

3.2 Electron microscopy study

To examine the morphological evolution, we recorded the scanning electron microscopy (SEM) images of the samples. Fig. 2a shows the SEM image of sample $NiFe_2O_4$-3 prepared at the hydrothermal aging time of 3 h, which is dominated by highly populated spherical particles of sizes below 15 nm. The SEM image of $NiFe_2O_4$-4 prepared at the hydrothermal aging time of 4 h also shows similar morphology and sizes. This might indicate that the hydrothermal aging time does not have much
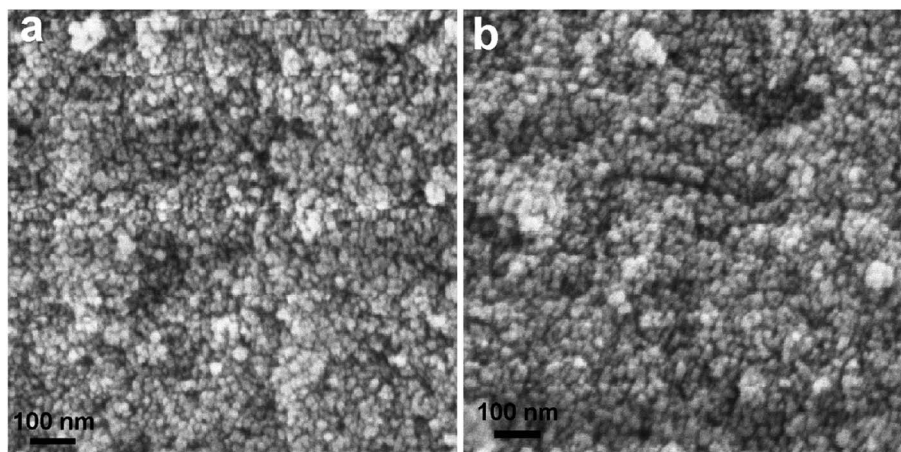
Fig. 2 FESEM images of the as-prepared $NiFe_2O_4$ NPs: (a) sample $NiFe_2O_4$-3 and (b) sample $NiFe_2O_4$-4.

influence on the morphology and size of the products. Srivastava *et al.* also reported the formation of spherical $NiFe_2O_4$ NPs of sizes 15–20 nm by a hydrothermal method at 160 °C for 15 h.[4] Abu-Dief *et al.* reported the synthesis of spherical $NiFe_2O_4$ NPs of an average size of 5 nm by the hydrothermal method at 180 °C for 24 h in presence of PEG.[8] Ganesh *et al.* observed the formation of clusters of sheets of $NiFe_2O_4$ of average crystallite size of 16 nm from the respective salts in an aqueous medium by a hydrothermal method performed at 130 °C for 12 h in presence of PVP.[42] The comparison of the results indicated that

in the absence of any additive, nearly monodisperse $NiFe_2O_4$ NPs can be obtained within a shorter time. The energy dispersive X-ray (EDX) spectroscopy analysis confirmed the presence of elemental Ni, Fe, and O in the atomic ratio of approximately 1 : 2 : 4 in both the samples (Fig. S1 in the ESI†).

Further to study the morphological evolution, transmission electron microscopy (TEM) images were recorded from the samples. The TEM image recorded from sample $NiFe_2O_4$-3 (Fig. 3a) further confirmed the presence of spherical NPs those are mostly aggregated. This might be due to the absence of any
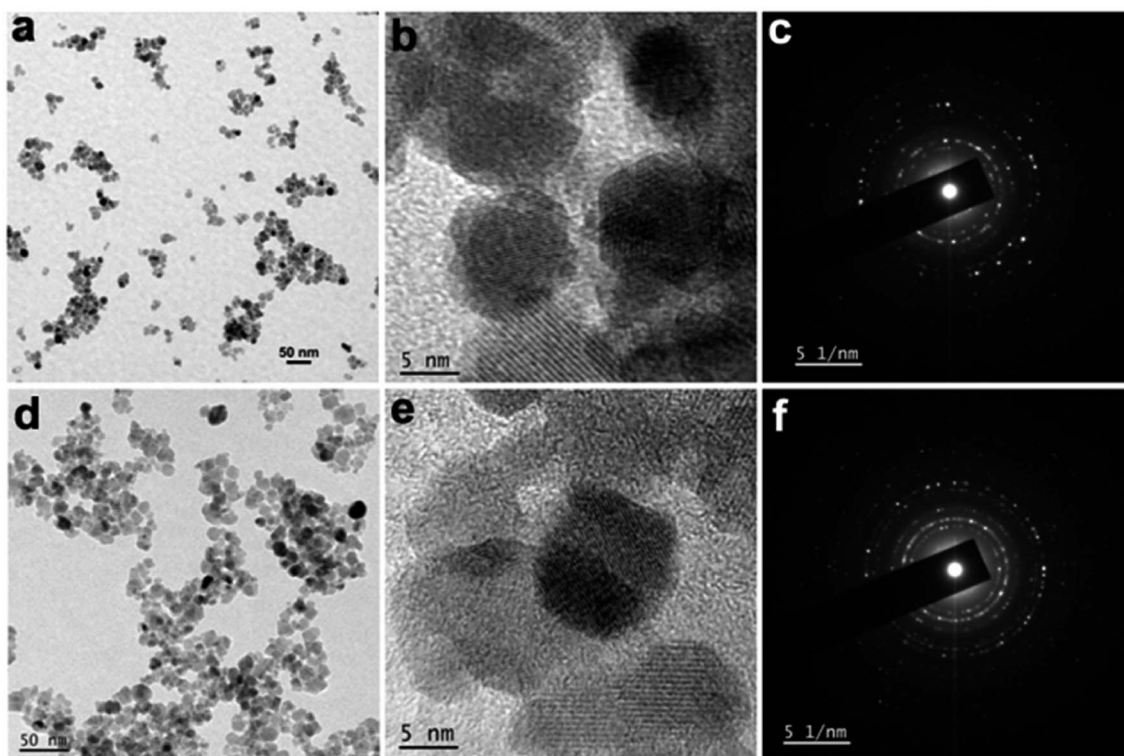

Fig. 3 TEM images of the as-prepared $NiFe_2O_4$ NPs: (a) TEM image, (b) HRTEM image, and (c) SAED pattern recorded from sample $NiFe_2O_4$-3 and (d) TEM image, (e) HRTEM image, and (f) SAED pattern recorded from sample $NiFe_2O_4$-4.

stabilizer or magnetic properties of the particles. The high-resolution TEM (HRTEM) image recorded from a portion (Fig. 3b) showed the presence of well-resolved lattice fringes with a d space value of 0.3 nm. This value corresponds to the (220) lattice plane in $NiFe_2O_4$. The selected area electron diffraction (SAED) study (Fig. 3c) revealed the presence of bright spots superimposed on a ring pattern confirming that the $NiFe_2O_4$ NPs are polycrystalline. The TEM image recorded from sample $NiFe_2O_4$-4 (Fig. 3d) also shows similar structural evolution as observed in sample $NiFe_2O_4$-3. In this case, the particles are more uniform compared to the previous one. The HRTEM image and SAED pattern also show similar characteristics as observed in sample $NiFe_2O_4$-3. The mean size of $NiFe_2O_4$ NPs for both the samples was calculated from TEM micrographs considering 100 particles (Fig. S2 in the ESI†). The mean sizes of $NiFe_2O_4$ NPs are 11.3 and 10.2 nm respectively for samples $NiFe_2O_4$-3 and $NiFe_2O_4$-4. A slight decrease in the particle size in sample $NiFe_2O_4$-4 might be attributed to the high hydrothermal aging time. Further, the average size obtained from TEM is slightly larger than the crystallite sizes of $NiFe_2O_4$ obtained from XRD results.

3.3 Magnetic property study

The hysteresis curve of the $NiFe_2O_4$ NPs was investigated using a vibrating sample magnetometer (VSM) at room temperature (300 K). The hysteresis curves of $NiFe_2O_4$ samples are shown in Fig. 4a. The $NiFe_2O_4$ NPs in both the samples exhibit super-paramagnetic behavior with the saturation magnetic moment (M_s) of 0.6 emu and without magnetic hysteresis loop, coercivity (H_c), and remanent magnetization (M_r). A similar observation was also noticed in the magnetic properties of $NiFe_2O_4$ NPs in sample $NiFe_2O_4$-4 which is a characteristic of super-para-magnetism.[43] The obtained saturation magnetization (M_s) value is lower than the values of bulk $NiFe_2O_4$ particles reported

elsewhere.[11] Super-paramagnetic behavior arises from the fact that when a magnetic field is applied, the NPs need to overcome the thermal barrier to align themselves with the direction of the field and above T_B due to thermal energy, this barrier is overcome.

The temperature-dependent magnetization of $NiFe_2O_4$ NPs was studied from zero field cooling-field cooling (ZFC-FC) measurements. For the ZFC-FC measurements, the sample was cooled down to 5 K in zero fields and the magnetization was recorded as the sample was heated to 300 K in an applied field of 500 Oe. Then, the sample was cooled to 5 K under an applied field of 500 Oe and the magnetization was recorded as the sample was heated to 300 K in the same field. The ZFC-FC curves of $NiFe_2O_4$ NPs are shown in Fig. 4b that exhibited a sharp divergence below 150 K with blocking temperatures (T_B) around 75 and 58 K respectively for samples $NiFe_2O_4$-3 and $NiFe_2O_4$-4. That is, the sample of $NiFe_2O_4$ NPs has a maximum in ZFC measurements and constant moments below T_B for FC measurements. This was due to the blocking of magnetic moments because of the presence of anisotropy. Such divergence of the magnetization below the blocking temperature in the ZFC-FC measurements is due to the existence of the energy barriers of magnetic anisotropy and the slow relaxation of the particles below the blocking temperature. This magnetic anisotropy energy barrier is the key to superparamagnetic relaxation.

3.4 X-ray photoelectron spectroscopy study

To study the elemental composition and the oxidation states of the elements present in the synthesized product, we analyzed the sample $NiFe_2O_4$-4 by X-ray photoelectron spectroscopy (XPS). A typical survey scan XPS spectrum present in Fig. 5a shows the presence of elements O 1s, Ni 2p, and Fe 2p. The high-resolution XPS spectrum of the core level Fe 2p
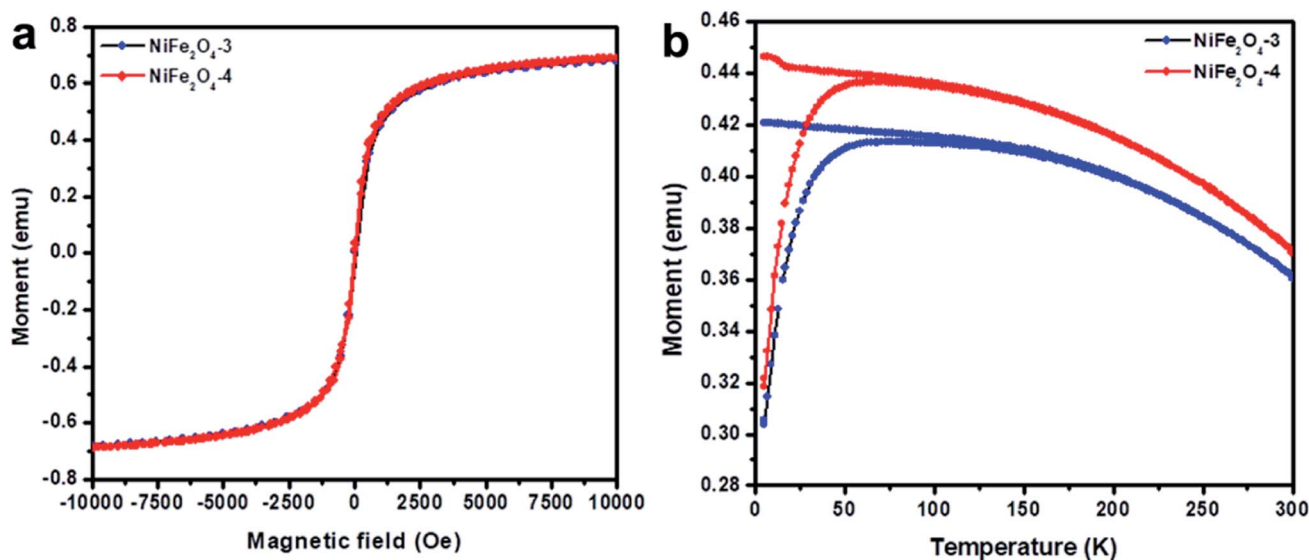

Fig. 4 (a) Magnetic hysteresis curves (M vs. H) of samples $NiFe_2O_4$-3 and $NiFe_2O_4$-4 at 300 K and (b) temperature dependence of magnetization of samples $NiFe_2O_4$-3 and $NiFe_2O_4$-4 measured under field-cooled (FC) and zero-field-cooled (ZFC) conditions at an applied field of 500 Oe.
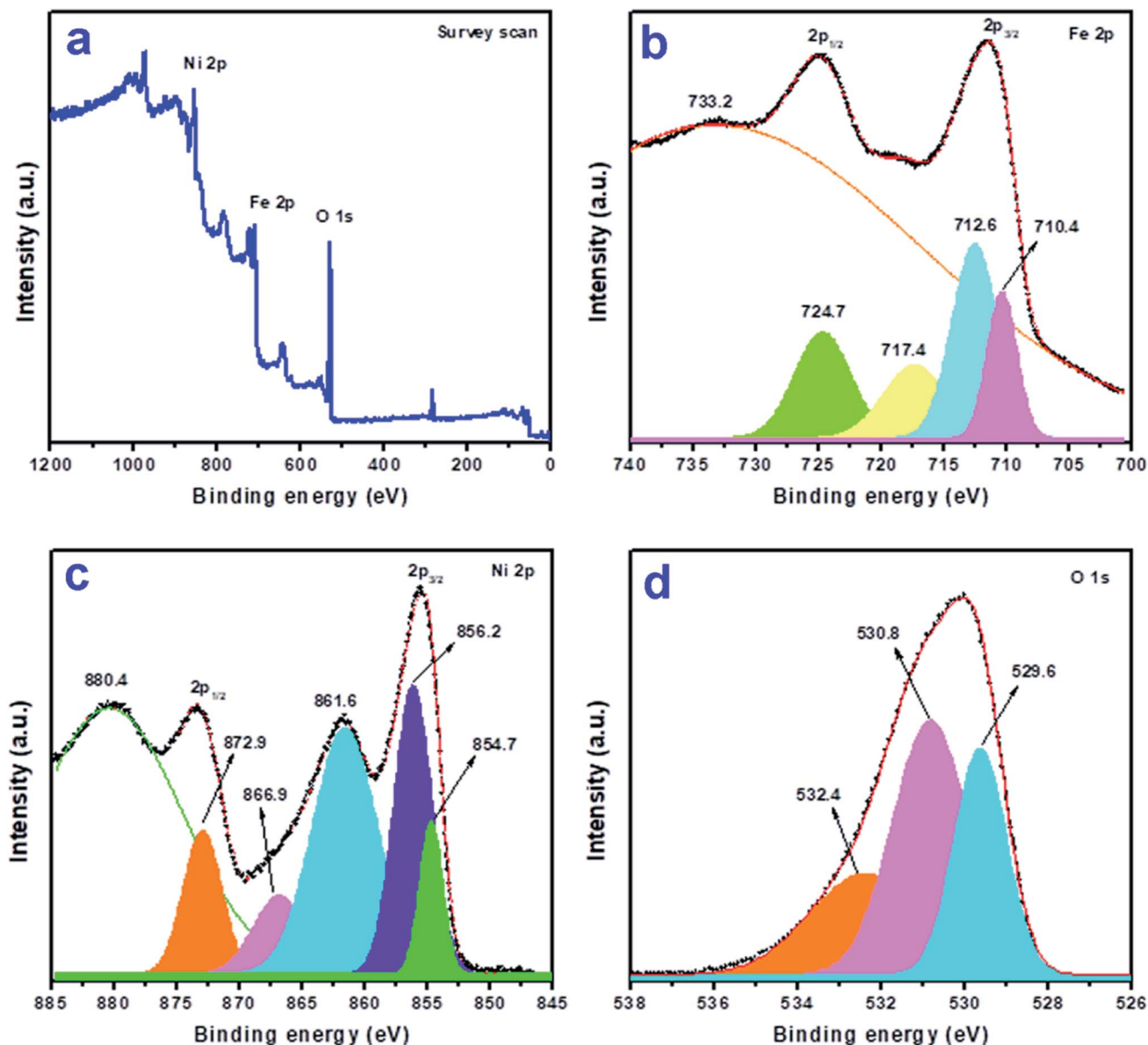
Fig. 5   X-ray photoelectron spectra of sample NiFe$_2$O$_4$-4: (a) survey scan, and (b) Fe 2p, (c) Ni 2p, and (d) O 1s regions.

region (Fig. 5b) shows two broad peaks at a binding energy of 724.9 eV (Fe 2p$_{1/2}$) and 711.5 eV (Fe 2p$_{3/2}$) with a satellite peak of Fe 2p$_{3/2}$ at around ~718.2 eV. These peaks correspond to the presence of Fe in the Fe(III) state in the product.[44] The presence of a satellite peak further supports the absence of the Fe$_3$O$_4$ phase in the composite. The Fe 2p$_{3/2}$ peak can further be fitted into two peaks at ~712.6 and ~710.4 eV which corresponds to the presence of Fe^{3+} ions in both octahedral and tetrahedral sites of NiFe$_2$O$_4$ respectively.[44] These observations further indicate that NiFe$_2$O$_4$ has a partial inverse spinel structure. Fig. 5c shows the high-resolution XPS spectrum of core level Ni 2p where two peaks were observed at 873.4 (Ni 2p$_{1/2}$) and 855.5 (Ni 2p$_{3/2}$) which are accompanied by another satellite peak at 861.6 eV. The Ni 2p$_{3/2}$ peak can further be fitted into two peaks at ~856.2 and ~854.7 eV which reveals the presence of two

non-equivalent bonds due to two types of lattice sites, i.e. tetrahedral and octahedral sites of NiFe$_2$O$_4$.[44] Fig. 5d shows the O 1s core-level spectrum, where three peaks were observed at 529.6, 530.8, and 532.4 eV in the fitted curve. The peak found at 529.6 eV is due to O^{2-} in the NiFe$_2$O$_4$ crystal lattice, whereas the peak at 530.8 is due to the chemisorbed oxygen associated with the surface adsorbed hydroxyl groups. The peak at binding energy 532.4 eV is attributed to the presence of water. A similar observation was reported earlier for NiFe$_2$O$_4$ thin films deposited on a quartz substrate deposited by radiofrequency magnetron sputtering.[45]

3.5   Oxidation of benzyl alcohol

To investigate the catalytic activity of prepared NiFe$_2$O$_4$ NPs, oxidation of benzyl alcohol was chosen. For the selection of

Table 1 Optimization of reaction conditions for the oxidation of benzyl alcohol in terms of solvent and oxidant[a]

$$CH_2OH \xrightarrow[\text{Solvent; 60 °C}]{\text{NiFe}_2\text{O}_4\text{; Oxidant}} CHO$$
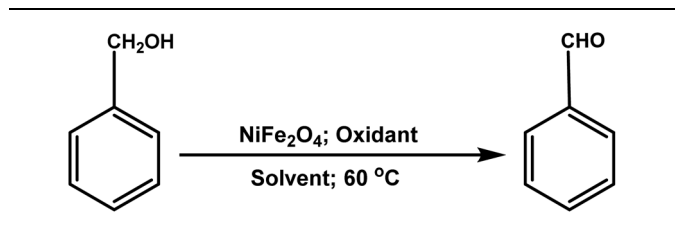
Entry	Solvent (mL)	Oxidant (mL)	Time (h)	Yield[c] (%)
1	—	O_2	6	Trace
2	—	H_2O_2 (0.5)	6	Trace
3	—	TBHP (0.05)	6	30
4[b]	—	TBHP (0.05)	6	Trace
5	C_2H_5OH (3.0)	TBHP (0.05)	6	Trace
6	CH_3OH (3.0)	TBHP (0.05)	6	15
7	2-Propanol (3.0)	TBHP (0.05)	6	42
8	CH_3CN (3.0)	TBHP (0.05)	3	85
9	H_2O (3.0)	TBHP (0.05)	6	Trace

[a] Benzyl alcohol = 1.0 mmol; catalyst = 10 mg (0.04 mmol). [b] No catalyst was used. [c] Isolated yield.

Table 2 Optimization of temperature, catalyst loading, and oxidant amount[a]

$$CH_2OH \xrightarrow[\text{CH}_3\text{CN; Heat}]{\text{NiFe}_2\text{O}_4\text{; TBHP}} CHO$$
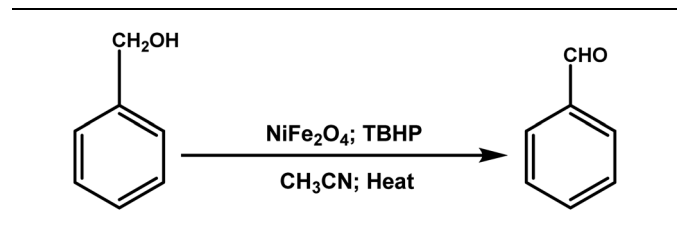
Entry	NiFe$_2$O$_4$ (mg)	TBHP (mL)	Temperature (°C)	Time (h)	Yield[b] (%)
1	10	0.05	110	3	87
2	10	0.05	60	3	85
3	10	0.05	50	3	73
4	10	0.05	40	3	55
5	10	0.05	rt	24	~20
6	5	0.05	60	3	60
7	15	0.05	60	3	85
8	20	0.05	60	3	85
9	10	0.01	60	3	52
10	10	0.03	60	3	70
11	10	0.1	60	3	60

[a] Reaction conditions: benzyl alcohol: 1 mmol. [b] Isolated yield.

oxidants, we tried first the oxidation of benzyl alcohol using different mild oxidants such as O_2, H_2O_2, and TBHP in the absence of any solvent. The use of molecular O_2 and H_2O_2 shows no significant conversion over a considerable time at 60 °C when 10 mg catalyst was used (Table 1; entry 1 and 2). The ineffectiveness of H_2O_2 in this system might be due to the possible decomposition of H_2O_2 over ferrite catalysts as reported earlier.[46] We observed that the system offers satisfactory results with TBHP (Table 1; entry 3). So, TBHP was used as an oxidant for the catalytic oxidation of benzyl alcohol. We also tried to investigate whether the reaction can be performed without a catalyst which produced a trace amount of product

that undergoes further oxidation to benzoic acid (Table 1; entry 4). This result revealed the usefulness of a catalyst for the oxidation of benzyl alcohol using TBHP as the oxidant at 60 °C. In the next assessment, the activity of the prepared catalyst was studied under different solvent atmospheres. So, we performed a set of reactions in the presence of different solvents such as ethanol, methanol, 2-propanol, acetonitrile, and water (Table 1, entry 5 to 9). Surprisingly in acetonitrile medium maximum activity of the catalyst was observed at 60 °C (Table 1, entry 8). The reaction achieved a conversion yield of 85% in 3 h. Polar

Table 3 Comparison of the efficiency of the current catalyst in the oxidation of benzyl alcohol to benzaldehyde with a few reported ferrite and non-ferrite catalysts

Entry	Catalyst (Amount)	Oxidant	Temperature (°C)	Solvent	Time (h)	Conversion (%)	Ref.
1	CoFe$_2$O$_4$ NPs	H_2O_2	110	—	5 h	>99	40
2	Supported NiFe$_2$O$_4$	O_2	80	Acetonitrile	—	77	36
3	NiFe$_2$O$_4$	TBHP	120 (MW)	—	2 h	46.2	48
4	CoFe$_2$O$_4$	TBHP	120 (MW)	—	2 h	88.9	48
5	Nano CoFe$_2$O$_4$	Oxone	rt	Water	20 min	93	37
6	CuFe$_2$O$_4$	O_2/TEMPO	100	Water	24 h	95	38
7	CoFe$_2$O$_4$@SiO$_2$	H_2O_2	rt	Water	6 h	51.2	49
8	Nano-functionalized NiFe$_2$O$_4$	H_2O_2	80	Acetonitrile	7 h	82.4	39
9	PEG-NiFe$_2$O$_4$ NPs	H_5IO_6	rt	Water	1.5 h	98	16
10	ZrO$_x$-MnCO$_3$/HRG nanocomposites	O_2	100	Toluene	4 min	~99	29
11	La$_{0.95}$Ce$_{0.05}$MnO$_3$	O_2	120	Toluene	12 h	40	32
12	Au/Sm-CeO$_2$	O_2	90	Toluene	3 h	27.4	21
13	Polyoxometalate-based catalyst PW$_4$/DAIL/MIL-100(Fe)	TBHP	100	Chloroform	6 h	92	33
14	MnO$_2$ NPs (calcined)	TBHP	110	Alcohol	24 h	89	34
15	Ce$_{0.8}$Zr$_{0.2}$O$_2$	TBHP	120	—	4 h	92.5	50
16	NiFe$_2$O$_4$ NPs	TBHP	60	Acetonitrile	3 h	85	This work

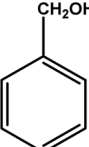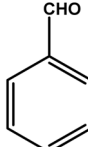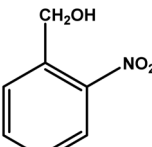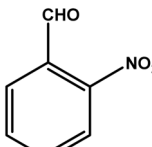**Table 4** Catalytic performance in the oxidation of benzylic and aliphatic alcohols[a]
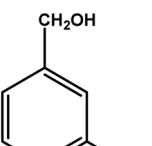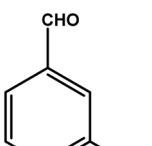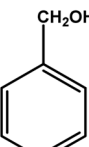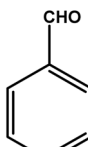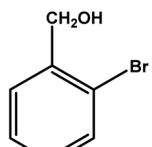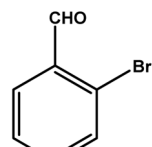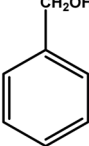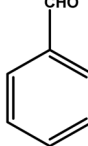
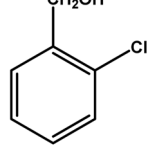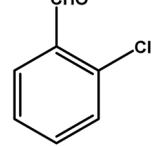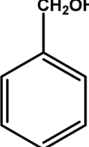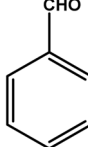| Entry	Alcohol	Product	Time (h)	Conversion[b] (%)	Specific activity (mmol g^{-1} h^{-1})	TON[c]	TOF[d] (h^{-1})
1			3	85	28.3	21.25	7.1
2			3	76	25.3	19.0	6.3
3			3	70	23.3	17.5	5.8
4			3	88	29.3	22.0	7.3
5			3.5	75	21.4	18.75	5.3
6			2	88	44.0	22.0	11.0
7			4	68	17.0	17.0	4.3
8			3	81	27.0	20.25	6.8

Nanoscale Advances

Table 4 (Contd.)

Entry	Alcohol	Product	Time (h)	Conversion[b] (%)	Specific activity (mmol g^{-1} h^{-1})	TON[c]	TOF[d] (h^{-1})
9	CH$_2$OH (4-OCH$_3$ benzyl alcohol)	CHO (4-OCH$_3$ benzaldehyde)	3	79	26.3	19.75	6.6
10	H$_3$C–(CH$_2$)$_5$–CH(OH)–CH$_3$	No reaction	24 (observation)	—	—	—	—
11	cyclohexanol (OH)	cyclohexanone (O)	18–24	Trace amount	—	—	—
12	HS–(CH$_2$)$_2$–CH$_2$OH	No reaction	24 (observation)	—	—	—	—
13	HS–(CH$_2$)$_5$–CH$_2$OH	HS–(CH$_2$)$_5$–CHO	12–24	~30	—	—	—

[a] Reaction conditions: benzyl alcohol: 1 mmol; TBHP: 0.5 mmol; NiFe$_2$O$_4$: 10 mg; solvent: CH$_3$CN; temperature: 60 °C. [b] Isolated yield. [c] TON: turnover number = number of moles of substrate consumed/number of moles of catalyst. [d] TOF: turnover frequency = TON/time of reaction in h.

and polar protic solvents like water and ethanol showed no satisfactory conversion (Table 1, entry 5, and 9), while methanol and 2-propanol offered a conversion of 15 and 42% yield respectively (Table 1, entry 6 and 7). So, we consider acetonitrile to be the effective solvent for the proposed conversion for the remaining study. The formation of the product was initially confirmed by the FTIR spectra (Fig. S3 in the ESI†). In the FTIR spectrum of pure benzyl alcohol, the broadband located at 3325.6 cm^{-1} could be attributed to the O–H stretching. The band shows peaks at 2878.2 cm^{-1} and 1452.9 cm^{-1} which are attributed to the C–H stretching and C–O–H peak respectively, whereas, in the spectrum of the product, an intense peak located at 1733.1 cm^{-1} could be observed which is attributed to the C=O stretching of benzaldehyde. The peaks at 2850.2 and 2920.9 cm^{-1} are associated with C–H stretching of the aldehyde respectively. The band located at 2959.2 cm^{-1} is attributed to the C–H aromatic stretching of the aldehyde.

To investigate the effect of temperature on the catalytic activity, we varied the temperature from room temperature to 110 °C (Table 2, entry 1–5). We observed that under similar reaction conditions the best yield of 87% was achieved at 110 °C in 3 h (Table 2, entry 1). However, the use of such a high temperature violates the rule of green chemistry and so the study is believed to be irrelevant. Optimizing and reducing the temperature to 60 °C with the same reaction condition showed a conversion with an 85% yield in 3 h (Table 2, entry 2). Further reduction of temperature to 50 and 40 °C slowed down the

conversion and the calculated yield was found to be 73 and 55% respectively after 3 h (Table 2, entry 3, 4). When the reaction was carried out at room temperature (26 °C), nearly 20% conversion was observed after 24 h (Table 2, entry 5). So the best temperature was chosen as 60 °C for the remaining study. In the next step, we optimized the reaction for the catalyst loading (Table 2, entry 6–8) and observed that 5 mg (0.02 mmol) of the NiFe$_2$O$_4$ NP catalyst produces a conversion with a 60% yield under similar reaction conditions. When the catalyst loading was further increased to 10, 15, and 20 mg, conversion with 85% yield was obtained at 60 °C in 3 h (Table 2). So, for the next assessment, we fixed the catalyst loading at 10 mg (0.04 mmol). Further to find the minimum amount of oxidant required for satisfactory conversion, we varied the amount of oxidant from 0.01 mL (0.08 mmol) to 0.1 mL (0.8 mmol) (Table 2, entry 9–11). We observed that 0.05 mL (0.4 mmol) of TBHP is sufficient for the maximum conversion (Table 2, entry 2).

It is well known that t-BuOOH mediated reactions proceed via a free radical mechanism. To prove the fact, we carried out a reaction in the presence of a radical quencher, hydroquinone which is an effective free radical scavenger for TBHP as reported earlier.[47] So, a set of reactions in the presence of hydroquinone (0.5 mmol) were performed keeping all other reaction parameters fixed as the parent reaction. As expected, we observed that the reaction is inhibited in the presence of the radical quencher as no significant product formation was noticed after 3 h of reaction. This observation proved that the reaction proceeds

through the involvement of the radical intermediate. Further, to examine the efficiency and capability of the present protocol, the result of the current study is compared with other related ferrite and non-ferrite based catalyst systems (Table 3). The comparative study revealed the effectiveness of the current catalyst system in the selective oxidation of benzyl alcohol to benzaldehyde under mild reaction conditions. Also, it can be seen that most of the catalysts required support which played a major role in the enhanced activity of the catalyst. However, the present catalyst system attained almost similar activity without any support materials.

To find the general applicability and the effectiveness of the TBHP/$NiFe_2O_4$ catalytic system, oxidations of various substituted benzyl alcohols and a few aliphatic and heteroatomic alcohols were performed under the optimized

conditions and the results are shown in Table 4. It can be seen from Table 4 that the *p*-substituted electron-withdrawing group (–NO_2, –Cl, and –Br) showed a greater yield of the product, whereas the *ortho* and *meta* substituted benzyl alcohols produce a lower yield. This might be due to the hindrance effect at the *ortho* position which causes slow oxidation of alcohol. On the other hand, the electron-donating group (–OCH_3) at the *p*-position of the ring also showed a low product formation in comparison with the electron-withdrawing group but a slightly better yield compared to the *ortho* and *para*-substituted electron-withdrawing groups. The specific catalytic activity, turnover number (TON), and turnover frequency (TOF) was found to be high for *p*-bromo benzyl alcohol. It was also observed that the current optimized conditions are too mild for the oxidation of aliphatic as well as heteroatomic alcohols (Table 4; entry 10–13) as a trace amount or no product formation was observed with these alcohols. The absence of conjugation in the β-position of the hydroxyl group might be the reason for this observation as reported earlier.[29] Also, the literature reports suggest that the oxidation of aliphatic alcohols is much more difficult than the oxidation of aromatic alcohols.[30,31,51,52] From these results, we conclude that the experimental conditions of the present catalyst system are not so favourable for the oxidation of aliphatic alcohols but very effective for selective oxidation of benzylic alcohols.

To check the reusability of the catalyst, first, we separated the catalyst magnetically using a bar magnet after the reaction, and the isolated products were purified by washing with water and a water–ethanol mixture to get rid of any organic reactants or products. The isolated mass was dried in an oven at 60 °C under vacuum overnight. The isolated catalyst was used for new batches of the oxidation reaction under identical reaction conditions as discussed above. The process of isolation, purification, and the catalysis reaction were repeated for 5 cycles. The performance of the reused catalyst was quite satisfactory up
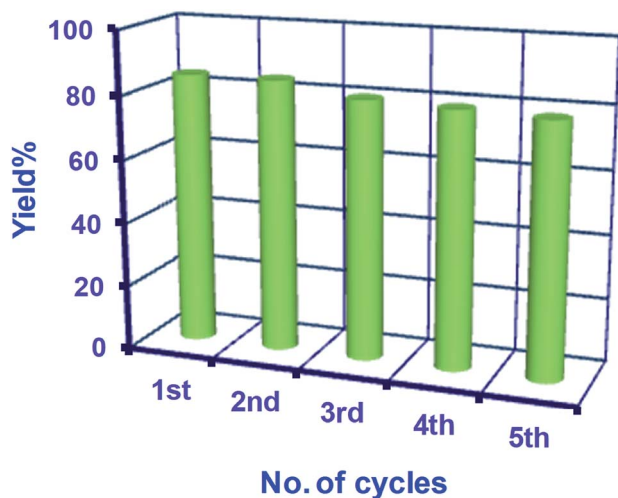

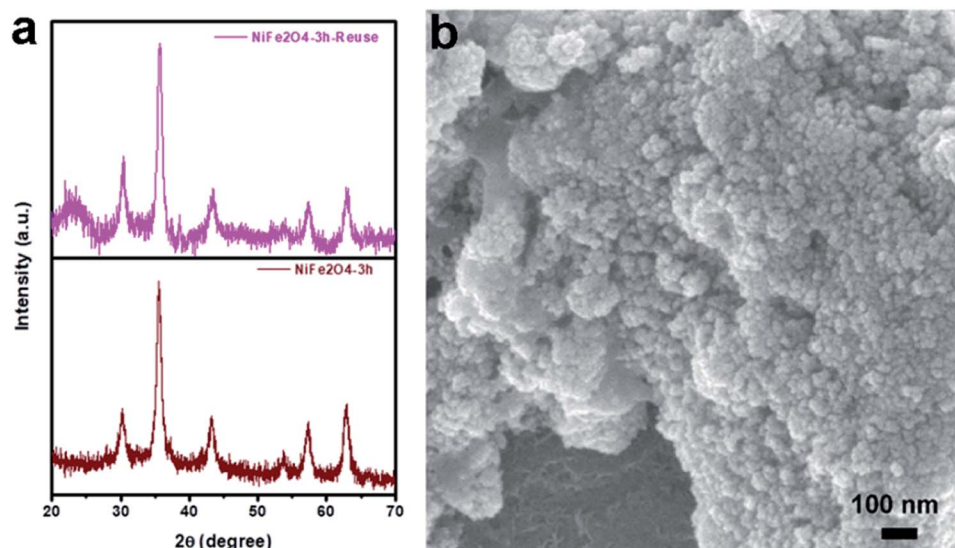**Fig. 6** Bar diagram showing the yield% of the product in different cycles of reuse of $NiFe_2O_4$ NPs.

Fig. 7 (a) XRD pattern and (b) SEM image of the recovered $NiFe_2O_4$ NPs after catalysis.

to the 5th cycle (Fig. 6). To study the fate of $NiFe_2O_4$ NPs during catalysis, the solid catalyst was isolated after the first cycle of reaction and dried at 60 °C under vacuum for further characterization. The XRD pattern of the used $NiFe_2O_4$ NPs exhibited similar crystalline properties with the nascent $NiFe_2O_4$ NPs (Fig. 7a). No major change in the crystalline properties was observed due to catalysis, although background noise could be observed in the XRD pattern. This might be due to the low quantity of the recovered sample. Also, the SEM image of the recovered sample (Fig. 7b) shows the presence of uniformly distributed spherical $NiFe_2O_4$ NPs. The results confirmed the stability of the sample during the catalysis.

4. Conclusion

Spherical $NiFe_2O_4$ NPs of sizes below 12 nm have been prepared by a precipitation method coupled with hydrothermal aging in water. The formed $NiFe_2O_4$ NPs are pure and highly crystalline possessing cubic structures. The hydrothermal aging time does not have any influence on the particle size and morphology. The $NiFe_2O_4$ NPs exhibit super-paramagnetic behavior with the saturation magnetic moment (Ms) of 0.6 emu without any magnetic hysteresis loop, coercivity (H_c), and remnant magnetization (M_r). These ferrite NPs exhibit excellent catalytic activity in the selective oxidation of benzyl alcohol and substituted benzyl alcohol under ambient conditions with 100% selectivity. Being magnetic, these ferrite NPs are easily separable from the reaction mixture with a simple bar magnet and are reusable up to five cycles without loss of catalytic activity.

Conflicts of interest

There are no conflicts to declare.

Acknowledgements

References

1 M. Sugimoto, The past, present, and future of ferrites, *J. Am. Ceram. Soc.*, 1999, **82**, 269–280.

2 N. Gupta, P. Jain, R. Rana and S. Shrivastava, Current development in synthesis and characterization of nickel ferrite nanoparticle, *Mater. Today: Proc.*, 2017, **4**, 342–349.

3 A. Šutka, R. Pärna, T. Käämbre and V. Kisand, Synthesis of p-type and n-type nickel ferrites and associated electrical properties, *Phys. B*, 2015, **456**, 232–236.

4 M. Srivastava, S. Chaubey and A. K. Ojha, Investigation on size dependent structural and magnetic behavior of nickel ferrite nanoparticles prepared by sol–gel and hydrothermal methods, *Mater. Chem. Phys.*, 2009, **118**, 174–180.

5 X. Lasheras, M. Insausti, I. Gil de Muro, E. Garaio, F. Plazaola, M. Moros, L. De Matteis, J. M. de la Fuente and L. Lezama, Chemical synthesis and magnetic properties of monodisperse nickel ferrite nanoparticles for biomedical applications, *J. Phys. Chem. C*, 2016, **120**, 3492–3500.

6 I. Sharifi, H. Shokrollahi and S. Amiri, Ferrite-based magnetic nanofluids used in hyperthermia applications, *J. Magn. Magn. Mater.*, 2012, **324**, 903–915.

7 E. Umut, M. Coşkun, F. Pineider, D. Berti and H. Güngüneş, Nickel ferrite nanoparticles for simultaneous use in magnetic resonance imaging and magnetic fluid hyperthermia, *J. Colloid Interface Sci.*, 2019, **550**, 199–209.

8 A. M. Abu-Dief, I. F. Nassar and W. H. Elsayed, Magnetic $NiFe_2O_4$ nanoparticles: Efficient, heterogeneous and reusable catalyst for synthesis of acetylferrocene chalcones and their anti-tumour activity, *Appl. Organomet. Chem.*, 2016, **30**, 917–923.

9 B. Atashkar, A. Rostami, A. Rostami and M. A. Zolfigol, $NiFe_2O_4$ as a magnetically recoverable nanocatalyst for odourless C-S bond formation via the cleavage of C–O bond in the presence of S_8 under mild and green conditions, *Appl. Organomet. Chem.*, 2019, **33**, e4691.

10 M. M. Bućko and K. Haberko, Hydrothermal synthesis of nickel ferrite powders, their properties and sintering, *J. Eur. Ceram. Soc.*, 2007, **27**, 723–727.

11 J. Zhang, J. Shi and M. Gong, Synthesis of magnetic nickel spinel ferrite nanospheres by a reverse emulsion-assisted hydrothermal process, *J. Solid State Chem.*, 2009, **182**, 2135–2140.

12 J. Huo and M. Wei, Characterization and magnetic properties of nanocrystalline nickel ferrite synthesized by hydrothermal method, *Mater. Lett.*, 2009, **63**, 1183–1184.

13 W. Shen, L. Zhang, B. Zhao, Y. Du and X. Zhou, Growth mechanism of octahedral like nickel ferrite crystals prepared by modified hydrothermal method and morphology dependent magnetic performance, *Ceram. Int.*, 2018, **44**, 9809–9815.

14 G. Kesavan, N. Nataraj, S.-M. Chen and L.-H. Lin, Hydrothermal synthesis of $NiFe_2O_4$ nanoparticles as an efficient electrocatalyst for the electrochemical detection of bisphenol A, *New J. Chem.*, 2020, **44**, 7698–7707.

15 M. Safaei, H. Beitollahi and M. R. Shishehbore, Synthesis and characterization of $NiFe_2O_4$ nanoparticles using the hydrothermal method as magnetic catalysts for electrochemical detection of norepinephrine in the presence of folic acid, *J. Chin. Chem. Soc.*, 2019, **66**, 1597–1603.

16 B. Paul, D. D. Purkayastha and S. S. Dhar, Size-controlled synthesis of $NiFe_2O_4$ nanospheres via a PEG assisted hydrothermal route and their catalytic properties in oxidation of alcohols by periodic acid, *Appl. Surf. Sci.*, 2016, **370**, 469–475.

17 O. Karaagac, S. Atmaca and H. Kockar, A facile method to synthesize nickel ferrite nanoparticles: Parameter effect, *J. Supercond. Novel Magn.*, 2017, **30**, 2359–2369.

18 H. Li, H.-z. Wu and G.-x. Xiao, Effects of synthetic conditions on particle size and magnetic properties of NiFe$_2$O$_4$, *Powder Technol.*, 2010, **198**, 157–166.

19 M. Y. Rafique, M. Ellahi, M. Z. Iqbal, Q.-u.-a. Javed and L. Pan, Gram scale synthesis of single crystalline nano-octahedron of NiFe$_2$O$_4$: Magnetic and optical properties, *Mater. Lett.*, 2016, **162**, 269–272.

20 K. Nejati and R. Zabihi, Preparation and magnetic properties of nano size nickel ferrite particles using hydrothermal method, *Chem. Cent. J.*, 2012, **6**, 23.

21 S. Mandal, K. K. Bando, C. Santra, S. Maity, O. O. James, D. Mehta and B. Chowdhury, Sm-CeO$_2$ supported gold nanoparticle catalyst for benzyl alcohol oxidation using molecular O$_2$, *Appl. Catal., A*, 2013, **452**, 94–104.

22 D. Kahlich, U. Wiechern and J. Lindner, *Propylene oxide; ullmann's encyclopedia of industrial chemistry*, Wiley-VCH Verlag GmbH & Co., 2000.

23 A. Patel and S. Pathan, Solvent free selective oxidation of styrene and benzyl alcohol to benzaldehyde over an eco-friendly and reusable catalyst, undecamolybdophosphate supported onto neutral alumina, *Ind. Eng. Chem. Res.*, 2012, **51**, 732–740.

24 G. Zhan, Y. Hong, F. Lu, A.-R. Ibrahim, M. Du, D. Sun, J. Huang, Q. Li and J. Li, Kinetics of liquid phase oxidation of benzyl alcohol with hydrogen peroxide over bio-reduced Tu/TS-1 catalysts, *J. Mol. Catal. A: Chem.*, 2013, **366**, 215–221.

25 C. Wiener and O. Pittet Alan, Process for preparing natural benzaldehyde and acetaldehyde, natural benzaldehyde and acetaldehyde compositions, products produced thereby and organoleptic utilities therefor, US Pat. US 4617419 A, 1986.

26 M. Kantham, P. Shreekanth, K. Rao, T. Kumar, B. C. Rao, and B. Choudhury, Selective liquid phase air oxidation of toluene catalysed by composite catalytic system, Patent Appl. US6743952B2, 2003.

27 J. Chai, H. Chong, S. Wang, S. Yang, M. Wu and M. Zhu, Controlling the selectivity of catalytic oxidation of styrene over nanocluster catalysts, *RSC Adv.*, 2016, **6**, 111399–111405.

28 M. N. Kopylovich, A. P. C. Ribeiro, E. C. B. A. Alegria, N. M. R. Martins, L. M. D. R. S. Martins and A. J. L. Pombeiro, in *Advances in organometallic chemistry*, ed. P. J. Pérez, Academic Press, 2015, vol. 63, pp. 91–174.

29 M. E. Assal, M. R. Shaik, M. Kuniyil, M. Khan, A. Al-Warthan, M. R. H. Siddiqui, S. M. A. Khan, W. Tremel, M. N. Tahir and S. F. Adil, A highly reduced graphene oxide/ZrO$_x$–MnCO$_3$ or –Mn$_2$O$_3$ nanocomposite as an efficient catalyst for selective aerial oxidation of benzylic alcohols, *RSC Adv.*, 2017, **7**, 55336–55349.

30 M. E. Assal, M. R. Shaik, M. Kuniyil, M. Khan, A. Y. Alzahrani, A. Al-Warthan, M. R. H. Siddiqui and S. F. Adil, Mixed zinc/manganese on highly reduced graphene oxide: A highly active nanocomposite catalyst for aerial oxidation of benzylic alcohols, *Catalysts*, 2017, **7**, 391.

31 M. E. Assal, M. Kuniyil, M. R. Shaik, M. Khan, A. Al-Warthan, M. R. H. Siddiqui and S. F. Adil, Synthesis, characterization, and relative study on the catalytic activity of zinc oxide nanoparticles doped MnCO$_3$, –MnO$_2$, and –Mn$_2$O$_3$ nanocomposites for aerial oxidation of alcohols, *J. Chem.*, 2017, **2017**, 2937108.

32 A. A. Ansari, N. Ahmad, M. Alam, S. F. Adil, S. M. Ramay, A. Albadri, A. Ahmad, A. M. Al-Enizi, B. F. Alrayes, M. E. Assal and A. A. Alwarthan, Physico-chemical properties and catalytic activity of the sol-gel prepared Ce-ion doped LaMnO$_3$ perovskites, *Sci. Rep.*, 2019, **9**, 7747.

33 S. Abednatanzi, A. Abbasi and M. Masteri-Farahani, Immobilization of catalytically active polyoxotungstate into ionic liquid-modified MIL-100(Fe): A recyclable catalyst for selective oxidation of benzyl alcohol, *Catal. Commun.*, 2017, **96**, 6–10.

34 F. Gaspar and C. D. Nunes, Selective catalytic oxidation of benzyl alcohol by MoO$_2$ nanoparticles, *Catalysts*, 2020, **10**, 265.

35 M. B. Gawande, A. Rathi, I. D. Nogueira, C. A. A. Ghumman, N. Bundaleski, O. M. N. D. Teodoro and P. S. Branco, A recyclable ferrite–Co magnetic nanocatalyst for the oxidation of alcohols to carbonyl compounds, *ChemPlusChem*, 2012, 77, 865–871.

36 R. Saranya, R. A. Raj, M. S. AlSalhi and S. Devanesan, Dependence of catalytic activity of nanocrystalline nickel ferrite on its structural, morphological, optical, and magnetic properties in aerobic oxidation of benzyl alcohol, *J. Supercond. Novel Magn.*, 2018, **31**, 1219–1225.

37 F. Sadri, A. Ramazani, A. Massoudi, M. Khoobi, V. Azizkhani, R. Tarasi, L. Dolatyari and B.-K. Min, Magnetic CoFe$_2$O$_4$ nanoparticles as an efficient catalyst for the oxidation of alcohols to carbonyl compounds in the presence of oxone as an oxidant, *Bull. Korean Chem. Soc.*, 2014, **35**, 2029–2032.

38 X. Zhu, D. Yang, W. Wei, M. Jiang, L. Li, X. Zhu, J. You and H. Wang, Magnetic copper ferrite nanoparticles/TEMPO catalyzed selective oxidation of activated alcohols to aldehydes under ligand- and base-free conditions in water, *RSC Adv.*, 2014, **4**, 64930–64935.

39 P. B. Bhat and B. R. Bhat, Magnetically retrievable nickel hydroxide functionalised AFe$_2$O$_4$ (A = Mn, Ni) spinel nanocatalyst for alcohol oxidation, *Appl. Nanosci.*, 2016, **6**, 425–435.

40 M. Nasrollahzadeh, M. Bagherzadeh and H. Karimi, Preparation, characterization and catalytic activity of CoFe$_2$O$_4$ nanoparticles as a magnetically recoverable catalyst for selective oxidation of benzyl alcohol to benzaldehyde and reduction of organic dyes, *J. Colloid Interface Sci.*, 2016, **465**, 271–278.

41 P. Sivakumar, R. Ramesh, A. Ramanand, S. Ponnusamy and C. Muthamizhchelvan, Preparation and properties of nickel ferrite (NiFe$_2$O$_4$) nanoparticles via sol–gel auto-combustion method, *Mater. Res. Bull.*, 2011, **46**, 2204–2207.

42 K. Ganesh, N. Nandini, S.-M. Chen and L.-H. Lin, Hydrothermal synthesis of NiFe$_2$O$_4$ nanoparticles as an efficient electrocatalyst for the electrochemical detection of bisphenol a, *New J. Chem.*, 2020, **44**, 7698–7707.

43 P. Deb, A. Basumallick, P. Chatterjee and S. P. Sengupta, Preparation of α-Fe$_2$O$_3$ nanoparticles from a nonaqueous precursor medium, *Scr. Mater.*, 2001, **45**, 341–346.

44 R. S. Yadav, J. Havlica, J. Masilko, L. Kalina, J. Wasserbauer, M. Hajdúchová, V. Enev, I. Kuřitka and Z. Kožáková, Effects of annealing temperature variation on the evolution of structural and magnetic properties of $NiFe_2O_4$ nanoparticles synthesized by starch-assisted sol–gel auto-combustion method, *J. Magn. Magn. Mater.*, 2015, **394**, 439–447.

45 C. Solís, S. Somacescu, E. Palafox, M. Balaguer and J. M. Serra, Particular transport properties of $NiFe_2O_4$ thin films at high temperatures, *J. Phys. Chem. C*, 2014, **118**, 24266–24273.

46 P. Lahiri and S. K. Sengupta, Spinel ferrites as catalysts: A study on catalytic effect of coprecipitated ferrites on hydrogen peroxide decomposition, *Can. J. Chem.*, 1991, **69**, 33–36.

47 D. Waffel, B. Alkan, Q. Fu, Y.-T. Chen, S. Schmidt, C. Schulz, H. Wiggers, M. Muhler and B. Peng, Towards mechanistic understanding of liquid-phase cinnamyl alcohol oxidation with tert-butyl hydroperoxide over noble-metal-free $LaCo_{1-x}Fe_xO_3$ perovskites, *ChemPlusChem*, 2019, **84**, 1155–1163.

48 N. M. R. Martins, L. M. D. R. S. Martins, C. O. Amorim, V. S. Amaral and A. J. L. Pombeiro, Solvent-free microwave-induced oxidation of alcohols catalyzed by ferrite magnetic nanoparticles, *Catalysts*, 2017, **7**, 222.

49 J. Tan, X. B. Liu, W. F. Chen and Y. L. Hu, Synthesis of magnetically separable nanocatalyst $CoFe_2O_4@SiO_2@MIL-53(Fe)$ for highly efficient and selective oxidation of alcohols and benzylic compounds with hydrogen peroxide, *ChemistrySelect*, 2019, **4**, 8477–8481.

50 C. A. Akinnawo, N. Bingwa and R. Meijboom, Tailoring the surface properties of meso-CeO_2 for selective oxidation of benzyl alcohol, *Catal. Commun.*, 2020, **145**, 106115.

51 E. Assady, B. Yadollahi, M. Riahi Farsani and M. Moghadam, Zinc polyoxometalate on activated carbon: An efficient catalyst for selective oxidation of alcohols with hydrogen peroxide, *Appl. Organomet. Chem.*, 2015, **29**, 561–565.

52 S. Hasannia and B. Yadollahi, Zn–Al LDH nanostructures pillared by Fe substituted keggin type polyoxometalate: Synthesis, characterization and catalytic effect in green oxidation of alcohols, *Polyhedron*, 2015, **99**, 260–265.